Published by IOP Publishing for SISSA
Received: *December 12, 2008*
Accepted: *January 7, 2009*
Published: *March 9, 2009*

Pixel 2008 International Workshop
Fermilab, Batavia, IL, U.S.A.
23–26 September 2008

LSST sensor requirements and characterization of the prototype LSST CCDs

V. Radeka,[a] J. Frank,[a] J.C. Geary,[b] D.K. Gilmore,[c] I. Kotov,[a,1,2] P. O'Connor,[a] P. Takacs[a] and J.A. Tyson[d]

[a] *Brookhaven National Laboratory, Upton, NY 11973, U.S.A.*
[b] *Harvard-Smithsonian Center for Astrophysics, 60 Garden St., Cambridge, MA 02138, U.S.A.*
[c] *Stanford Linear Accelerator Center, Menlo Park, CA 94025, U.S.A.*
[d] *University of California, Davis, CA 95616, U.S.A.*

E-mail: kotov@bnl.gov

Abstract: LSST parameters are discussed and requirements on the LSST camera are presented. Characterization methods and results on a number of new devices produced specifically to address LSST's performance goals, including flatness, QE, full well capacity, linearity, dark current, read noise, CTE, and image persistence are presented. The results indicate that commercially produced, thick n-channel over-depleted CCDs can achieve excellent red response, high CTE, low dark current and satisfy LSST requirements with no evidence of persistent image artifacts. We will also report ongoing studies of mosaic assembly techniques to achieve chip-to-chip co-planarity, high fill factor, and thermal stability.

Keywords: Detectors for UV, visible and IR photons; Optics

[1] Corresponding author.

[2] This manuscript has been co-authored by employees of Brookhaven Science Associates, LLC. Portions of this work are supported by the Department of Energy under contract DE-AC02-76SF00515 with the Stanford Linear Accelerator Center, contract DE-AC02-98CH10886 with Brookhaven National Laboratory, and contract W-7405-ENG-48 with Lawrence Livermore National Laboratory. Additional funding comes from private donations, grants to universities, and in-kind support at Department of Energy laboratories and other LSSTC Institutional Members.

doi:10.1088/1748-0221/4/03/P03002

2009 JINST 4 P03002

Contents

1 Introduction

The Large Synoptic Survey Telescope, LSST, ambitious goal is a wider-deeper-faster survey. Wider means close to the whole sky coverage. The survey area will include 30,000 deg^2 and $\sim$ 20,000 deg^2 region will be observed $\sim$1000 times over a 10 year period. Deeper means that the single visit depth should reach to r$\sim$24 (5 sigma for point sources). Faster means that a single visit exposure time is less than 40 seconds. A survey with these parameters enables a wide range of science based on a sample of $\sim$3 billion lensing galaxies, 10 million supernovas, tracking of objects as small as $\sim$140 m etc. Some of the major science goals are: to probe Dark Energy and Dark Matter; take an inventory of the Solar System; map the Milky Way; and to explore the Transient Optical Sky.

The LSST is a ground based telescope. The image quality is limited by the atmosphere and telescope hardware should not degrade this level of the image quality. The atmosphere turbulence also limits the practical field-of-view of the telescope. The LSST field-of-view area is maximized to its practical limit 9.6 deg^2. The primary mirror size is driven by required survey depth (for adopted sky coverage and survey lifetime). As the result, LSST primary mirror effective diameter is 6.5 m (annulus with 8.4 m outer diameter). For given field-of-view and primary mirror sizes the needed focal plane diameter is $\sim$65 cm. For the required resolution this amounts to a 3.2 Giga pixels camera. The desirable wavelength range of interest covers visible and near infrared regions and extends from the edge of atmosphere absorption to silicon detection limit, 320-1050 nm. The LSST base line parameters [1] are summarized in table 1 and the optical design is illustrated in figure 1.

2009 JINST 4 P03002

Table 1. The LSST base line parameters.

Quantity	Design Specification
Optical configuration	3-mirror modified Paul-Baker
f-Ratio, aperture	f/1.234, 8.4 m
Field of view, etendue	9.6 deg^2, 318 m^{2}deg^2
Plate scale	0.2 arcsec/pixel
Pixel size, pixel count	10 μm, 3.2 Gigapixel
Wavelength coverage	320-1050 nm, ugrizy
Single visit depth	r$\sim$24
Single visit exposure time	30 sec (two 15 sec exposures)
Readout time	2 sec

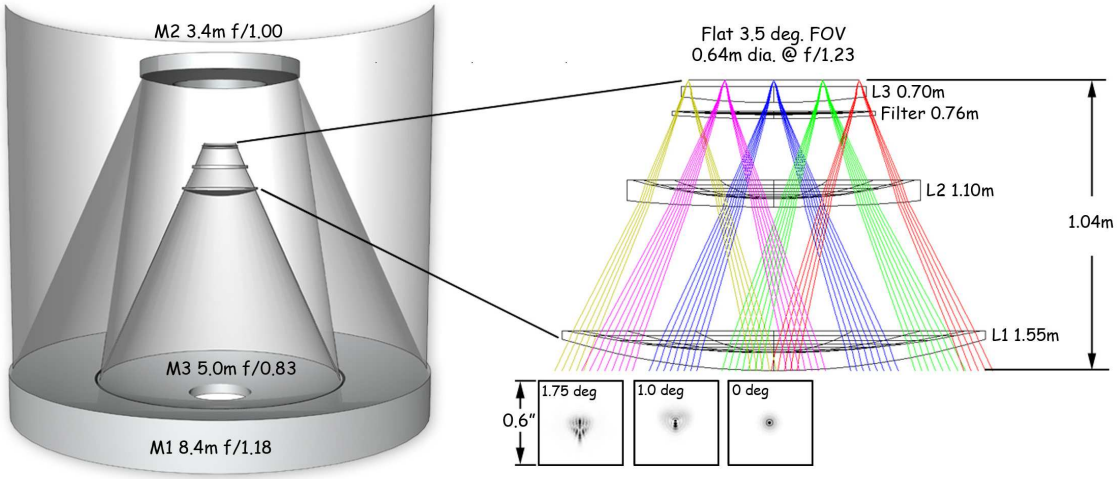

Figure 1. The LSST base line optical design. Primary M1 and tertiary M3 mirrors form a continuous compound surface.

2 LSST camera and sensor requirements, design optimization and prototype testing

To enable the wide-deep-fast survey, the LSST camera should be large, fast, with high quantum efficiency (QE) over the broad wavelength band and with low noise level. In addition, LSST's fast optics places tight tolerances on focal plane flatness. The well established technology based upon Charge Coupled Devices (CCD) was chosen for LSST focal plane sensors. But technological advances are needed to provide the required readout speed and achieve simultaneously high QE in near IR and small point spread function (PSF). The LSST camera requirements and needed technology advances are summarized in table 2.

Tradeoffs between different LSST requirements and design optimizations are discussed in the following sections (detailed discussions are also in [2]–[4]). A study program [5] was undertaken with several vendors to fabricate and test devices which address the challenging performance issues.

2009 JINST 4 P03002

Table 2. LSST sensor requirements.

Science driver	Technology Advance	Criterion
Broadband, high QE	Thick silicon, fully depleted	QE(1000nm) > 30%
	Transparent back contact	QE(400nm) > 40%
Seeing-limited image quality	Low charge diffusion	< 3.2μm rms
	Small pixel size	10μm (0.2")
	Low read noise	< 5 e- rms
	Low dark current	< 2 e-/pix/s
	Low persistence	$< 10^{-4}$
	High full well	> 90,000 e-
	Flat silicon surface	< 5μm p-v
	TTP-controlled package	< 6.5μm over raft
High throughput	Multiport output	$(4K)^2$, 16 output
	High fill factor die & pkg	> 93%

These devices were tested at Brookhaven National Laboratory (BNL) in a CCD test facility. Results from the prototype devices are presented.

2.1 CCD test facility

A CCD test facility was set up in the Brookhaven National Laboratory Instrumentation Division. It consists of two separate test stations: one station for metrology and raft assembly tests and one station for CCD characterization. All equipment is controlled over GPIB, RS-232 or IEEE-1394. The primary instrumentation of the CCD characterization station includes:

- liquid nitrogen cooled Dewar with: 4" window; temperature controlled table for CCD mounting; Fe55 source "sweeper" which moves the source from behind the shield position over the CCD active area and back;
- CCD controller based on MMT Megacam readout electronics [6]. The readout rate for our measurements was fixed at 156 kpix/s. Communication with the Linux PC is by optical fiber interface [7];
- mono-chromatic flat field illuminator (Xe lamp, grating mono-chromator, 12" integrating sphere, photo diodes and filters);
- long working distance, diffraction limited, high N.A., 10x projector for focusing a laser light coming out of 4 micron fiber into sub-micron spot on the CCD surface;
- XYZ stack for projector positioning;
- voltage source, ammeters, temperature controller and vacuum gauges.

The remote telescope software RTS2 [8] is used to control measuring devices and orchestrate image taking. Software runs on a Linux PC platform. Scripts and automated analysis procedures were developed to perform complete CCD characterization and for in depth investigation of specific CCD characteristics. One example of the express analysis output, ^{55}Fe X-ray spectra with fit to K_α and K_β lines, is shown in figure 2.

2009 JINST 4 P03002

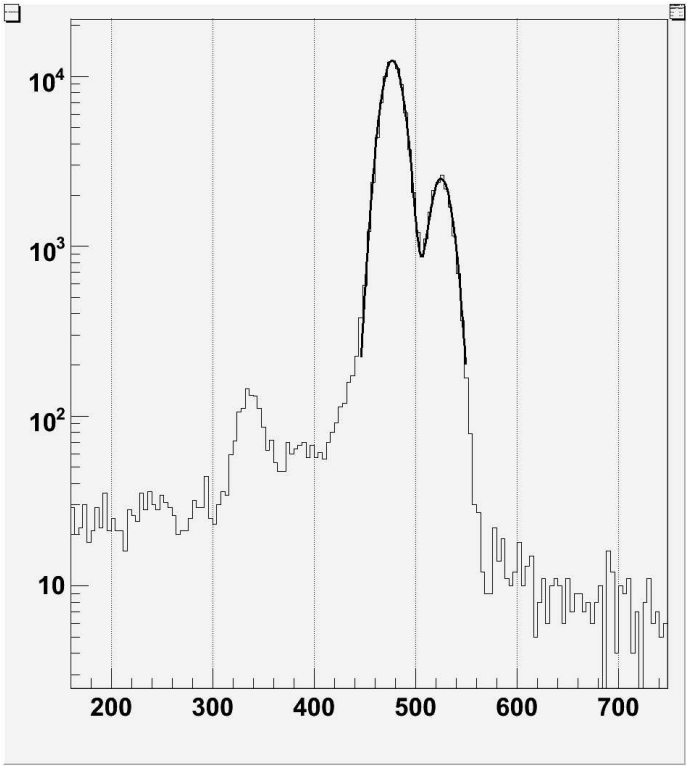

Figure 2. ^{55}Fe X-ray spectra with fit to K_α and K_β lines. Horizontal axis is cluster amplitude in adu and vertical is number of events.

The instrumentation of the metrology station includes gantry positioning system and optical con-focal displacement sensor Keyence LT-9030 for non-contact flatness measurements. The accuracy of the flatness measurement is presently limited by the non-idealities of the gantry to about 2μm.

2.2 QE and PSF

One of the major tradeoffs to balance is the tradeoff between QE and charge diffusion responsible for sensor contribution to the system PSF. To achieve high QE in red and near IR, sensor thickness should be at least comparable to the silicon absorption length for these wavelengths. The absorption length rapidly grows with the wavelength and at 1000 nm reaches $\sim$300 microns at 173K. Thus sensor thicknesses exceeding 100 microns are favorable for QE. On the other hand the charge diffusion and divergent optical beam of the telescope broadens PSF of a thick sensor. To balance the tradeoff between red QE and sensor PSF, an optimization study was performed [3]. An optimum with respect to both QE and PSF appears to be around 100 microns for sensor temperature $\sim$173K. The absorption length and in turn QE strongly depends on the temperature. Higher temperature increases QE while the effect on charge diffusion is minimal. But the thermally generated dark current and bright defects push toward cooler operating temperatures.

At the blue end of the LSST wavelength range the absorption length is a few microns. This requires a very shallow but highly doped layer to create a biased conductive window and is tech-

2009 JINST 4 P03002

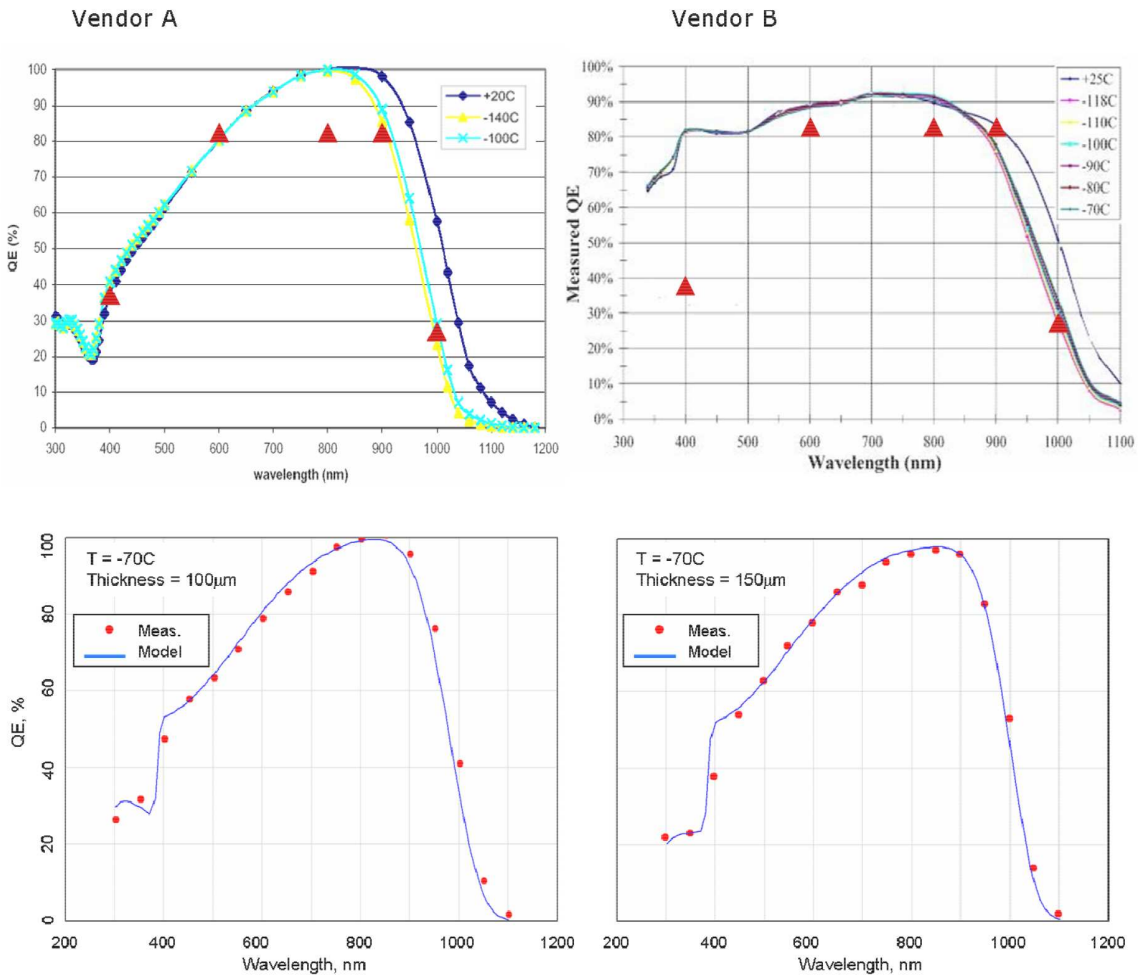

Figure 3. Quantum efficiency measured by vendors for 100 μm thick devices is shown in the top panels. Triangles are LSST requirements. Bottom panels show our measurements and modeled QE for vendor A devices. The model takes into account the absorption coefficient of silicon at -70°C from [9], the properties of the antireflection coating determined by ellipsometry and an assumed dead layer of 6nm at the entrance window.

nologically challenging.

QE was measured for study contract devices by taking flat field exposures over a wavelength range 300-1100 nm simultaneously with photon flux measurements by the monitor photodiode in the integrating sphere. Results for both 100 μm and 150 μm thick devices are shown in the bottom panels of figure 3. From CCD exposures the average number of electrons detected per pixel was determined; the average number of incident photons was calculated from photo diode readings. To calculate both quantities, gain and efficiency measurements are required. The photo diode came with factory calibration data and geometrical corrections were measured in situ. The CCD gain and charge transfer efficiency (CTE) were measured using ^{55}Fe data. After correction on CTE the CCD gain is determined from the fit similar to one shown in figure 2.

The change in position of the K_α and K_β lines depending on the number of serial or parallel

2009 JINST 4 P03002

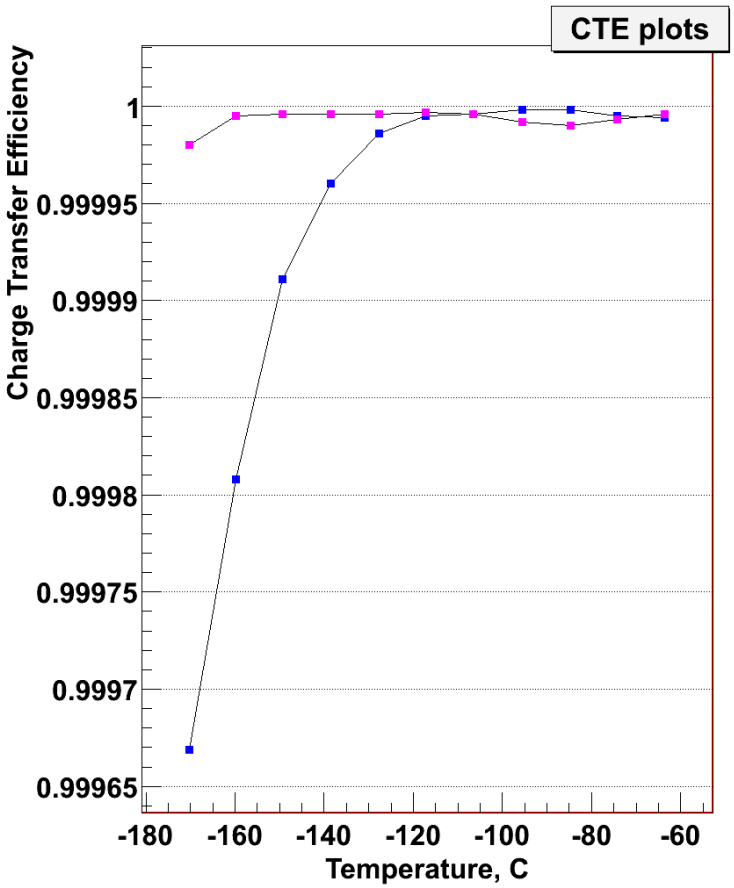

Figure 4. Charge Transfer Efficiency for 2K*4K device. Blue points are for serial transfer efficiency and magenta points are for parallel transfer.

transfers allows a measurement of charge transfer efficiencies. High CTE value is important to achieve bias free weak lensing shear measurements. LSST requires CTE to be higher than 0.99999 (five nines). The results of CTE measurements are shown in figure 4 for the temperature range -170°°C - -60°C.

Both serial and parallel transfer efficiencies exceed LSST requirements at temperatures warmer than -120°C. Clock levels and timing were at vendor recommended settings.

A single layer AR coating used by vendor A exceeds LSST QE minimum requirements in the major part of the wavelength band. Reproducibility of the QE measurements is better than 1% in the 400-900 nm wavelength range. Absolute accuracy is limited by uncertainties in gain determinations with photo diode gain uncertainty +/-5% (3σ level) dominating.

For PSF measurements, we are investigating different techniques: virtual knife edge (VKE), cosmic ray track width, x-ray cluster size, and Modulation Transfer Function (MTF). The VKE technique is most straightforward (for details see [10, 11]). The spot produced by the point projector is repeatedly imaged as it is scanned in 2μm steps in x or y. Integrating the flux in a fixed group of pixels through which the spot travels allows one to estimate the size and shape of the point spread function. The VKE profile is fitted to the error function to get an estimate of the PSF due to charge diffusion effects in the CCD.

2009 JINST 4 P03002

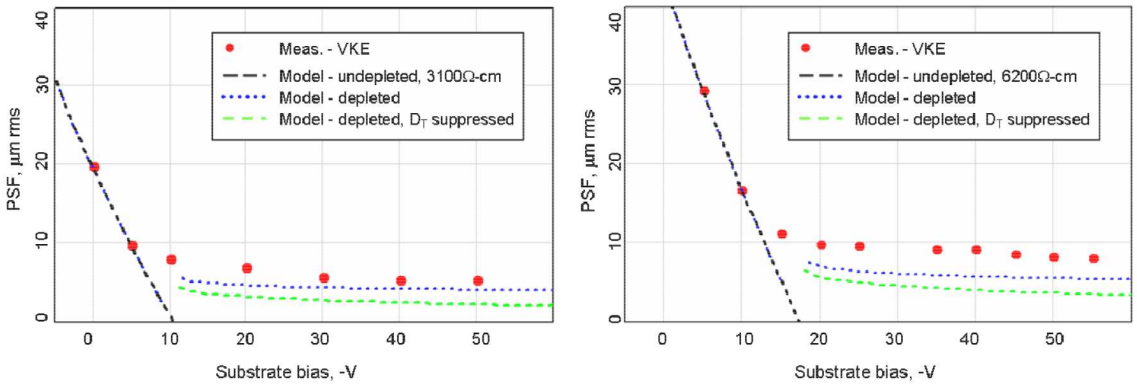

Figure 5. Point spread function measured by the virtual knife edge technique for samples 106-05 (left) and 107-01 (right).

The point spread function measured by the VKE technique is shown in figure 5 for two devices. Data for both samples were taken at 163K. By fitting the low-voltage portion of the curve the doping concentration, silicon thickness, and junction potential can be determined to be [4.1x10^{12}cm^{-3}; 95μm; and 18V] for 100 μm thick sample 106-05 and [2.1x10^{12}cm^{-3}; 150μm; and 18V] for 150 μm thick sample 107-01 respectively. As the voltage is made more negative the CCD becomes fully depleted and the PSF is determined by the diffusion of electrons. Figure 5 shows two curves for the PSF based on the known velocity-field relation for electrons in high-purity silicon [12]. The smaller PSF values assume that the transverse diffusion coefficient, D_T is suppressed at high fields according to the model of [13]. The analysis of systematic uncertainties in VKE measurements and PSF measurements using three other techniques are in progress. Initial results from those techniques show somewhat smaller PSF, in better agreement with the theory.

2.3 Readout speed, noise, dark current and defects

The effective depth of the single visit exposure increases with reduced noise (for given exposure time). The LSST science goals require the read noise r.m.s. to be below 5 electrons for 2 seconds full focal plane readout time. This is the practical limit achievable in the tradeoff between exposure efficiency (readout time is one component of the dead time for the telescope), noise degradation with increase of readout speed and sensor segmentation. The noise analysis of the source follower transistor [5] and noise measured on existing devices [14] shows that 5 e- noise level is achievable at readout speed of 500 kpix/s. The 4K*4K sensor thus requires sixteen 1 Mpix segments to be readout in parallel.

The dark current thermally generated inside a CCD is another important contribution to the system noise and has to be kept at the same level as readout noise. This translates into 2e-/pixel/s limit on the dark current. The dark current was measured for contract study devises and mean dark current dependence on the temperature is shown in figure 6. Dark current is measured by taking the slope of the signal versus exposure time linear fit for each pixel, in a series of dark runs. An example of pixel amplitude distribution at different exposure times for a series of 50°C temperature runs is shown in figure 7.

2009 JINST 4 P03002

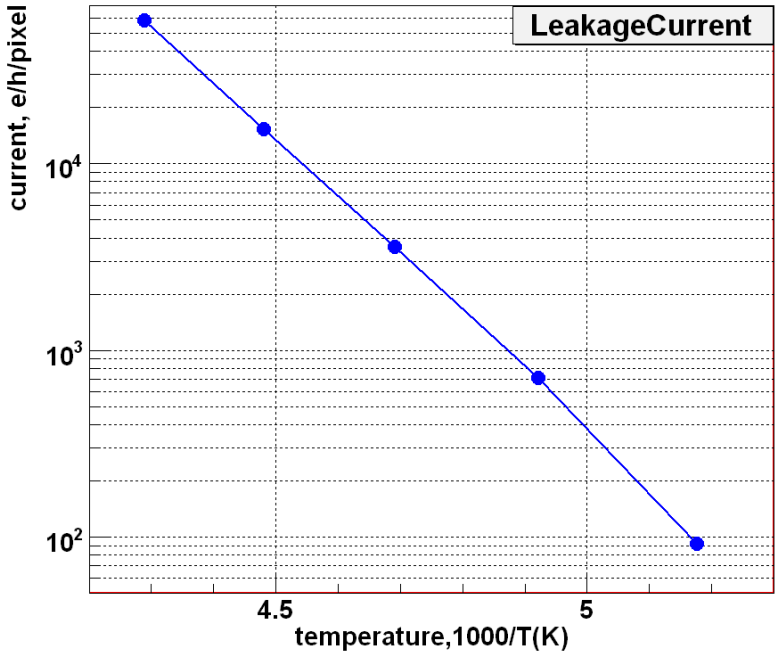

Figure 6. Dark current at different temperatures.

CCD defects reduce the usable CCD area and a 5% limit is set by LSST requirements. Bright defects are extinguished at lower temperature. Most study contract sensors were within this limit at operating temperatures up to -60°C.

2.4 Full well, linearity and persistent image

Figure 8 shows the sensor 106-06 response to flat field illumination at increasing exposure times. The full well (figure 8(a)) is about 300,000 electrons. Figure 8(b) shows that the response is linear to within 0.5% from zero to 90% of full well.

Study contract devices were tested for image persistence. The light coming out of 4 micron fiber coupled to the red laser was focused onto the surface of the CCD. The intensity and exposure time was adjusted to produce about 1/3 of full well in the brightest pixel. The exposure sequence, laser exposure followed by 20 laser-off exposures, was repeated sixteen times without moving the laser spot. As shown in figure 9, image persistence was less than 0.03%, with the measurement limited by signal to noise ratio.

3 Reference design, sensor and focal plane flatness

3.1 Reference design

A reference design for LSST sensors has been proposed based on the preceding design studies. As shown in figure 10, it is a 4K $\times$ 4K CCD fabricated on 100 μm thick, p-type silicon with a resistivity in the range 5–10 kΩ-cm. The CCD imaging area is divided into sixteen, 512 $\times$ 2048 pixel, independently read out segments. Each segment has a low power, low noise source

2009 JINST 4 P03002

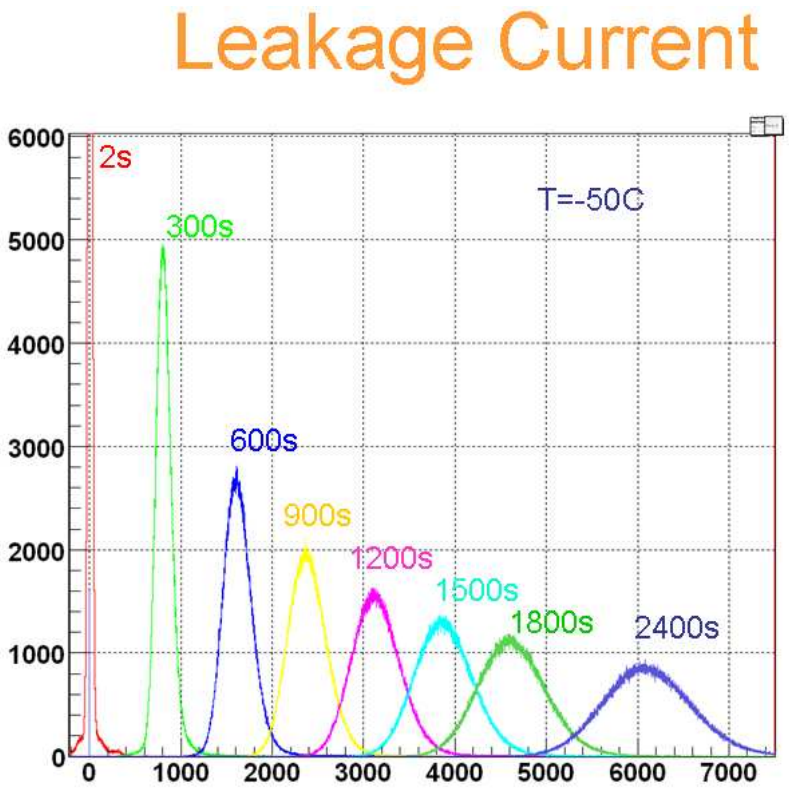

Figure 7. Pixel amplitude distribution in dark frames with different exposure times. Horizontal axis is amplitude in adu and vertical axis is number of pixels.

follower amplifier. An independent substrate bias voltage, applied from the front side of the device, biases the thin conductive window on the backside and results in a fully-depleted substrate under the imaging area with electric field of 5–10 kV/cm. Guard rings around the periphery provide a gradual lateral voltage gradient to the silicon die edge, which is at the same potential as the entrance window. Care must be taken to ensure that p-implanted regions on the front side are narrow enough to avoid forming conductive channels to the backside. Bond pads are arranged on two sides of the die and connect to traces on the package, which may incorporate bussing of common clocks and bias signals.

3.2 Flatness

A crude defocus model provides limits on the flatness tolerance. Figure 11 shows the normalized PSF as a function of displacement from best focus. The proposed allocation of flatness tolerance for the sensor surface, raft of nine sensors, and full focal plane of 189 sensors is shown.

At the chip level this involves packaging techniques to minimize warpage of the silicon die, and at the mosaic level careful assembly and metrology to achieve a high co-planarity of the sensor tiles.

Results of the flatness measurements for Vendor A devices are shown in figure 12. The departure from flatness is within LSST specifications over more than 96% of the imaging area for these

2009 JINST 4 P03002

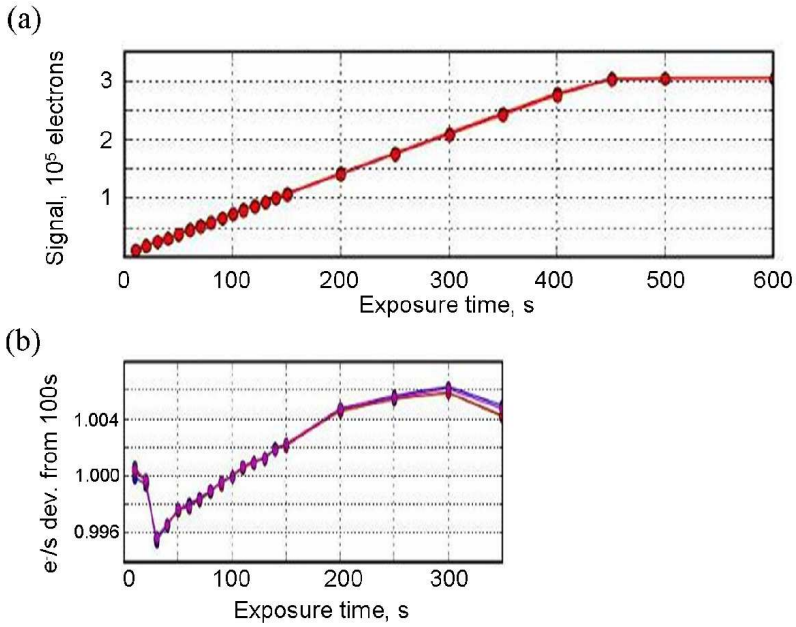

Figure 8. (a) Response to flat field illumination. (b) Slope normalized to the value at 100s. Response is linear up to 90% of full well.

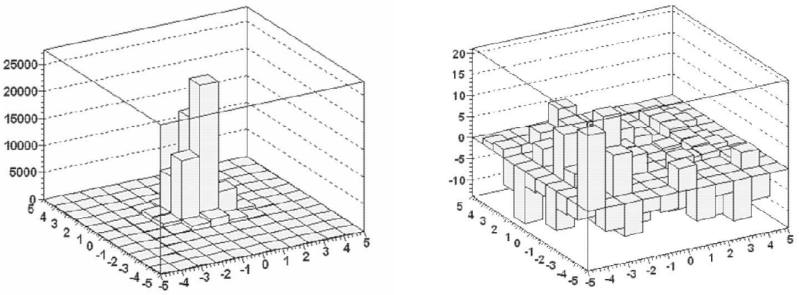

Figure 9. Absence of image persistence in n-channel CCD 106-05. Averages of 16 exposures are shown for the laser spot (left) and first exposure after laser turned off (right). There is no persistence image up to the level of measurements accuracy $3*10^{-4}$.

devices. One of Vendor B's devices has been measured and it exhibits a poorer flatness characteristic, with an r.m.s. deviation from plane about seven times larger than the devices from Vendor A. However, neither vendor made any special attempt to produce flat devices for this study program.

4 Summary and outlook

The LSST sensor study program has been an important step towards development of the advanced sensors needed to achieve the survey's ambitious science goals. Vendors participating in the study program have demonstrated viable approaches to producing devices having extended red response with 100μm-thick, fully-depleted silicon; transparent back window contact; low dark current; negligible image persistence; high full well; flat silicon surface; and multiport output for fast readout.

2009 JINST 4 P03002

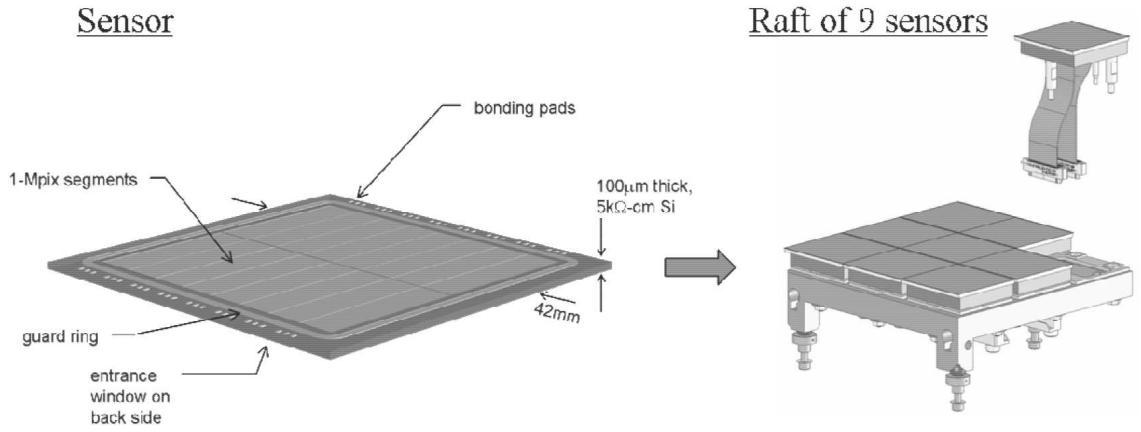

Figure 10. Sensor and raft reference designs.

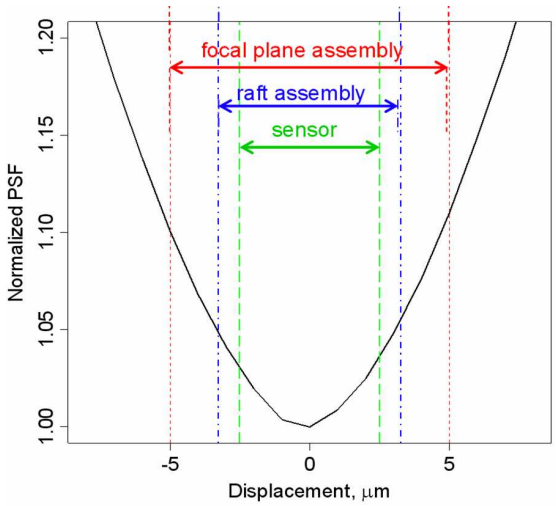

Figure 11. Estimated defocus for 550nm light, with allocation to sensor, raft, and full focal plane. A 3.2μm r.m.s. Gaussian PSF at optimum focus is assumed.

A characterization laboratory at BNL with fully automated image acquisition and analysis has verified the performance characteristics of the devices. The collaboration now plans to work with vendors to develop a full prototype meeting all critical LSST specifications that will allow procurement to begin in 2011.

Acknowledgments

This report was prepared as an account of work sponsored by an agency of the United States Government. Neither the United States Government nor any agency thereof, nor any of their employees, nor any of their contractors, subcontractors, or their employees, makes any warranty, express or implied, or assumes any legal liability or responsibility for the accuracy, completeness, or any third party's use or the results of such use of any information, apparatus, product, or process disclosed, or represents that its use would not infringe privately owned rights. Reference herein to

2009 JINST 4 P03002

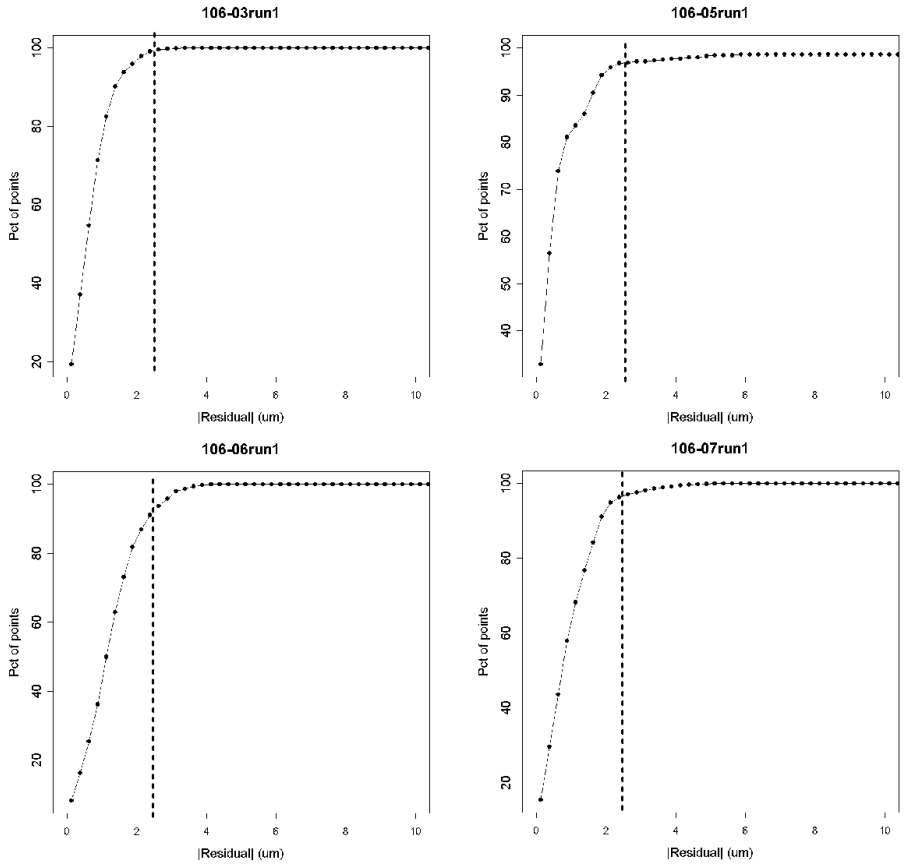

Figure 12. Flatness of Vendor A sensors.Plots show cumulative distribution of flatness (absolute value of residuals to best-fit plane). Vertical dashed line is LSST spec.

References

[1] Z. Ivezic et al., *LSST: from science drivers to reference design and anticipated data products*, arXiv:0805.2366.

[2] V. Radeka, *CCD and PIN-CMOS developments for large optical telescopes*, in *Proceedings of International Symposium on Detector Development for Particle, Astroparticle and Synchrotron Radiation Experiments (SNIC 2006)*, April 3–6 2006, Menlo Park, California [SNIC-2006-0005].

2009 JINST 4 P03002

[3] P. O'Connor et al., *Study of silicon thickness optimization for LSST*, *Proc. SPIE* **6276** (2006) 62761W.

[4] J.C. Geary et al., *The LSST Sensor technologies studies*, *Proc. SPIE* **6276** (2006) 627601.

[5] P. O'Connor et al., *Characterization of prototype LSST CCDs*, *Proc. SPIE* **7021** (2006) 702106.

[6] J.C. Geary and S. Amato, *Camera electronics for the 72-channel S.A.O. Megacam*, *Proc. SPIE* **3355** (1998) 539. J.C. Geary, *Signal processing for the SAO Megacam*, in *Further developments in scientific optical imaging*, M.B. Denton ed., Royal Society of Chemistry, Cambridge (2000) 18–23.

[7] PCI DV FOX, Engineering Design Team, Inc., www.edt.com.

[8] P. Kubanek et al., *Remote telescope system 2nd version*, *AIP Conf. Proc.* **727** (2004) 753.

[9] K. Rajkanan et al., *Absorption coefficient of silicon for solar cell calculations*, *Solid State Electrn.* **22** (1979) 793.

[10] A. Karcher et al., *Measurement of lateral charge diffusion in thick, fully depleted, back-illuminated CCDs*, *IEEE Trans. Nucl. Sci.* **51** (2004) 2231.

[11] J. Fairfield et al., *Reduced Charge Diffusion in Thick, Fully Depleted CCDs With Enhanced Red Sensitivity*, *IEEE Trans. Nucl. Sci.* **53** (2006) 3877.

[12] C. Canali, G. Majni, R. Minder, and G. Ottaviani, *Electron and Hole Drift Velocity Measurements in Silicon and Their Empirical Relation to Electric Field and Temperature*, *IEEE Trans. Electron Dev.* **22** (1975) 1045.

[13] V. Arora, *Drift diffusion and Einstein relation for electrons in silicon subjected to a high electric field*, *Appl. Phys. Lett.* **80** (2002) 3763.

[14] P. Jorden et. al., *Commercialisation of Full Depletion Scientific CCDs*, *Proc. SPIE* **6276** (2006) 627604.

2009 JINST 4 P03002